Influence of yaw-roll coupling on the behavior of a FPSO: an experimental and numerical investigation

Claudio Lugni[a,b], Marilena Greco[a,b], Odd Magnus Faltinsen[b]

[a] *CNR-INSEAN, The Italian Ship Model Basin, via di Vallerano 139, 00128 Roma - Italy.*
[b] *Centre for Autonomous Marine Operations and Systems (AMOS), Dept. of Marine Technology, NTNU, Trondheim - Norway.*

Abstract

An inconvenience in the experimental set-up of a FPSO in regular waves highlighted occurrence of parametric-roll events promoted by yaw-roll coupling and motivated a combined physical and numerical analysis on the relevance of this phenomenon on the roll resonance, as well as on the water shipping. The model tests examine the ship in head- and bow-sea waves in the zone of the first parametric resonance. Numerically, it is adopted a 3D Domain-Decomposition (DD) strategy combining a weakly-nonlinear potential-flow solver based on the weak-scatterer theory with a shallow-water approximation for the shipped liquid and with a bottom-slamming solution. Detailed comparisons against these and other seakeeping experiments validated the numerical method in its different aspects with global success.

At first, a 2-dof equivalent linearized yaw-roll coupled system is examined and the measurements are used to estimate hydrodynamic coefficients required to complete the mathematical model of the problem. Then the DD method is applied to verify the instability occurrence and compared against the experiments. From the analysis, the parametric-roll instability does not occur if all nonlinearities in the roll restoring load are not accounted for. However the amplitude of the resonant roll is affected by the coupling with the other degrees of freedom. Especially the coupling with yaw tends to increase the steady-state roll amplitude. It also affects the water shipping with the trend in reducing its severity for the vessel, this is opposite to the influence of the parametric roll in head-sea waves on the water on deck, as documented in Greco et al. (2014).

Keywords: Parametric roll, roll-yaw coupling, water on deck, experiments, weak-scatterer theory, nonlinear restoring, damping, instability.

1. Introduction

The importance of roll-yaw coupling is well known in quartering and following sea for high-speed vessels since it might lead to dynamic instability known as broaching, characterized by heading change towards beam-sea conditions and possible ship capsize. In this framework, a comprehensive description of the involved phenomena and the reference to relevant literature can be found *e.g.* in [1]. The importance of this coupling is less documented in bow-sea

*Corresponding author: Marilena Greco. Tel: +39 50299289; +47 73595440. E-mail address: marilena.greco@cnr.it; marilena.greco@ntnu.no.

conditions though examples have been recorded in the real life. Here this is examined in the context of dynamic instability for a FPSO ship. To the authors knowledge also this aspect has not been much documented previously however a lot of work has been done in the wider context of nonlinear ship motions and parametric roll. For example, a recent overview of studies connected with large roll motions is provided in [2].

This work is part of an ongoing comprehensive physical investigation on the behavior of Floating Production Storage and Offloading (FPSO) platforms in waves. In their common operational conditions they are at rest and weather-vaning, which means that head-sea waves are relevant for them.

Three-dimensional model tests were carried out on a FPSO ship at rest, without mooring-line systems, and interacting with regular head- and bow-sea waves. The experimental set-up was designed to allow only heave and pitch, or only heave, pitch and roll, while the other rigid motions were restrained. The main focus was on the investigation of the occurrence and features of water shipping, parametric-roll resonance and bottom slamming events in terms of incident-wave properties and induced body motions, and to assess the interactions among these different phenomena. Mutual influence between parametric-roll and water-on-deck phenomena were examined by [3] and [4] in head-sea conditions, i.e. heading angle $\beta = 180°$. It was found that in some conditions one of the two can be the cause of the other; that the roll resonance leads to a flow of the shipped water asymmetric with respect to the ship longitudinal axis and tends to increase the green-water loads; that the water on deck tends to increase the steady-state roll amplitude and can reduce or enlarge the duration of the transient phase of the ξ_4 time history.

Here the influence of motions coupling on the parametric roll and water shipping is examined, with main focus on yaw-roll coupling in bow-sea waves with $\beta = 175°$. Preliminary results are documented in [5]. The work is structured as follows: the experiments, in terms of model set-up, measurements and incident-wave conditions, are described in the next section; main features of the numerical model relevant for the present analysis are outlined in section 3; then the two research tools are compared and complementary used to carry on the physical investigation. A numerical study on a fishing vessel in regular waves showing a similar role of the yaw-roll coupling in the ship instability as discussed here is also examined. The last section is devoted to summarize the main findings.

2. Experiments

A detailed description of the model tests and information about error analysis can be found in [4]. Here the main features are outlined with emphasis on the measurements relevant for the physical investigation documented in section 4.

A FPSO model in scale 1:40 has been tested at the basin No. 2 (length x width x depth = 220 x 9 x 3.6 m) of CNR-INSEAN equipped with a flap wavemaker Kempf & Remmers hinged at a height of 1.8 m from the bottom. The ship model, its body plan and the main hydrostatic properties are provided in figure 1. The model was fixed to the carriage through a mechanical system which consists of a vertical shaft and a gimble (see left picture of figure 1). The shaft slides in a cylindrical bearing in order to keep free the heave motion and is connected to the model by means of a

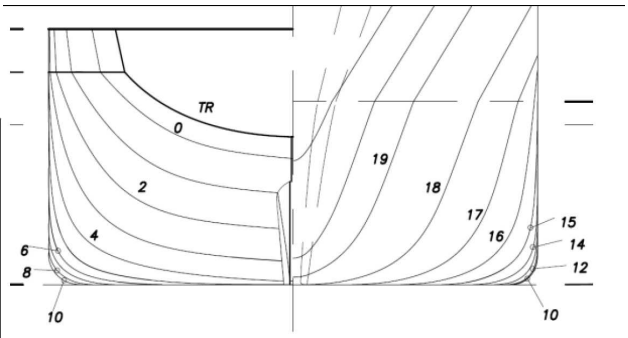

	Model sc.	Full sc.
Length (L)	4.22 m	168.8 m
Breadth (B)	0.81 m	32.4 m
Draft (D)	0.25 m	10.0 m
Displacement	663 kg	43493 t
Metacentric height (GM)	0.036 m	1.44 m
Pitch gyration radius (K_{yy})	0.27 L	0.27 L
Roll gyration radius (K_{xx})	0.37 B	0.37 B

Figure 1: Experimental set-up: FPSO model in scale 1:40 (left), body plan (right-top) and main hydrostatic properties at model and full scale (right-bottom).

gimble which allows free oscillations in pitch and roll. The remaining degrees of freedom were restrained in all tests. This arrangement was made to analyze water-on-deck and parametric-roll occurrence and features. The cylindrical shape of the shaft should block the yaw motion through a load cell but the arrangement did not work properly and so the vessel experienced yaw motion during the tests. Here, the focus is given on experimental cases where non-zero yaw motions occurred due to a slack in the shaft mechanism. This set-up inconvenience was in a way a fortunate event, since motivated the investigation of the yaw-roll coupling influence on instability occurrence.

The ship was tested at rest without mooring-line system and without bilge keels. The roll damping connected with the examined model and the vessel roll natural period were estimated through free-decay tests in calm-water conditions. This showed a 1-dof roll natural period $T_{4n0} = 2\pi/\omega_{4n0} \simeq 3.56$ s. Here the symbol T_{4n0} is used to stress that the natural period in roll T_{4n} can be modified by the coupling with other degrees of freedom when the latter are non zero, through cross-coupling added mass and restoring terms. In the following the uncoupled natural period of the roll is indicated as calm-water natural period. Using the free-decay recordings of the roll motion and modelling the ship as a 1-dof system in roll, an equivalent linear damping, which well approximates the roll damping mechanisms involved, has been identified as $B_{44,1}/(I_{44} + A_{44}) = 0.03$ s^{-1}. It corresponds to $B_{44,1} \simeq 0.0262 B_{44}^{crit}$, with B_{44}^{crit} the critical damping. This damping level is due to wave-radiation and viscous bare-hull contributions (see the body plan in the right-top sketch of figure 1) and is relatively low when compared with values expected for practical FPSOs, typically ranging between 0.05 and 0.15. The greater damping is due to bilge keels and mooring lines usually adopted and leading to additional contributions with nonlinear trend of the damping load with the roll speed.

Regular waves with heading angle of 180, 175 and 170 degrees were generated to reproduce conditions relevant for weather-vaning platforms, *i.e.* head or close-to-head sea conditions. The wavelength-to-ship length ratio λ/L has been set equal to 0.75, 1, 1.25, 1.5 and 2, and the incident-wave steepness kA varied between 0.1 and 0.25 with step 0.05. These wave parameters were chosen because relevant to examine occurrence and features of water shipping in terms of liquid evolution and induced loads, both as local pressures at seven positions along the deck centreline and of mid-ship bending moment. To this purpose a vertical superstructure was introduced on the deck (see left plot of figure 1) to simulate a deck house located in the bow area, consistently with arrangements for FPSOs operating in North sea. Converting the values of the examined λ/L into values of calm-water (uncoupled) roll natural frequency-to-excitation frequency ratio, ω_{4n0}/ω, we have a variation within [0.402,0.656]. It means that the chosen incident-wave conditions are in the region of first parametric resonance for the roll, corresponding to $\omega_{4n}/\omega = 0.5$. This is why the experiments allowed to investigate water-on-deck and parametric-roll phenomena and their mutual influence.

Different local and global measurements were performed during the tests. Among them, present physical analysis examines: the incident-wave elevation, the rigid ship motions, the 3D video recordings and the yaw moment acting on the shaft.

The evolution of the wave elevation in the tank was measured at two locations, approximately 5.7 and 34 m upstream of the ship Center of Gravity (CoG), using a Kenek finger probe and a capacitance wire probe, respectively. The Kenek is a non-intrusive sensor with an accuracy of 0.1 mm and a measure range of ±150mm. The used capacitance wave probe has an accuracy comparable with the wire diameter, i.e. 0.5 mm, and a linearity range of ±300 mm. In particular the farther probe (from CoG) measurements were used to assess the actual incident waves relative to the prescribed conditions by analyzing the recorded time histories after the initial transient and before waves reflected from the vessel could reach the probe. This check appeared to be relevant due to some problems identified in the wavemaker and solved after the experimental campaign. In the analysis the terms 'prescribed' and 'actual' will be used to distinguish between desired and achieved incident waves. The rigid ship motions were estimated with both an inertial (MOTAN) and an optical (Krypton) system to cross check the experimental conditions. In particular, the MOTAN measures the linear accelerations and the angular velocities of the rigid body and the motions are obtained from time integrations, while the Krypton measures directly the ship motions. The MOTAN has a resolution around 1 mm for the translational motions and 0.15 deg for the angular ones, while the corresponding accuracy errors for the Krypton are, respectively, less than 1 mm and less than 0.05 deg. The 3D video recordings were performed through a low-speed camera (with 25 fps) and used to document the ship behavior in waves from front and side views. The yaw moment acting on the shaft was measured with a torque sensor with an accuracy of ±0.5Nm.

A sample rate of 333 Hz was used to acquire the quantities analyzed in the present work. A common starting signal allows their synchronization with the camera systems.

Present physical analysis examines bow waves with $\beta = 175°$, using also comparison against pure head-sea conditions. Occurrence and features of parametric roll and water shipping as a function of incident waves and induced body motions are discussed, with focus on the relevance of yaw-roll coupling.

3. The numerical method

A detailed description of the adopted solver can be found in [6] and in [4]; here only the main features relevant for the present investigation are described. This is done to help understanding and gain insights when comparing numerical results against experiments, especially in terms of important parameters and physical phenomena involved.

A Domain-Decomposition (DD) strategy is used. It couples two local solvers, predicting the occurrence and induced loads of, respectively, water-on-deck and slamming phenomena, with a global seakeeping method for a six degree-of-freedom vessel. A sketch with the solver main features is given in figure 2.

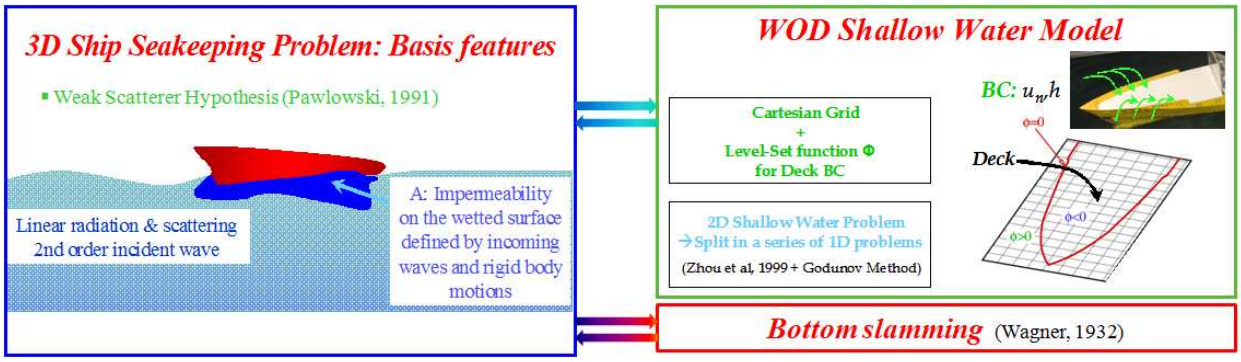

Figure 2: Main features of the Domain-Decomposition strategy.

The water-shipping occurrence is predicted by checking locally along the deck profile the freeboard exceedance and the entering flux of water. In particular, the freeboard exceedance is estimated as the local relative vertical motion between the waves (including the second-order incident waves and the linear radiation and diffracted waves) and the rigid body. The flux of water considers the local relative velocity between the incident waves and the ship. Once the event has been identified a water-on-deck solver is switched on and applied in time as long as water is on the deck. This models the global features of the most common water-on-deck scenario characterized by a dam-breaking type of flow onto the deck. Therefore the evolution of the shipped water is predicted within the shallow-water approximation solving the problem on a Cartesian grid fixed to the deck and using a splitting method to transform a 2D shallow-water problem along the deck plane into a sequence of 1D coupled problems along the main axes of the computational grid (see [7]). The one directional fluxes are found using an exact Riemann solver (Godunov's method, see *e.g.* [8]) but the temporal scheme is accurate to the first order. A level-set function (as in [9]) is used to identify the deck profile and possible superstructures and so to transfer the boundary conditions, in terms of water level and flow velocities, onto the computational-grid nodes.

The bottom slamming is identified using a modified Ochi's criterion, because the original Ochi's criterion was found to be too conservative in [6]. This new criterion was proposed in [6] and combines the Ochi's velocity criterion with a pressure condition. It requires the detection of a water-entry phase obtained through the check of the local relative vertical motion between the waves (including the second-order incident waves and the linear radiation and diffracted waves) and the rigid body. It also needs the estimation of the impact velocity, defined as local relative

vertical velocity between the incident waves and the ship, and the prediction of the slamming pressure to be compared with the pressure from the Bernoulli equation for the wave-body interaction problem not accounting for slamming. The slamming pressure is predicted by a local Wagner-type [10] solution. Once the slamming has been identified, this local solution is switched on at the hull positions where the slamming criterion is satisfied and this solution remains locally active as long as the slamming criterion applies.

The global 3D seakeeping solver uses the weak-scatterer hypothesis (see e.g. [11]), meaning that the incident waves and body motions are assumed large relative to the scattering and radiation effects and so the wavelength-to-ship length ratio must be sufficiently large. Nonlinearities are retained up to the second order for the incident waves and for Froude-Krylov and hydrostatic loads and a correction of the linear scattering and radiation loads is obtained by satisfying in time averagely the impermeability condition along the instantaneous wetted hull surface defined by the incident waves and the body motions.

The motion equations are solved in time domain with Cummins's approach [12] so to handle transient phenomena. Moreover nonlinear-load effects are also included, though strictly speaking this approach is valid for linear problems. It is assumed that the body weight is balanced by the mean buoyancy and the rigid-body motion equations are written along a body-fixed coordinate system with origin in the center of gravity. They involve convolution integrals connected with combined radiation and scattering loads since within the weak-scatterer approximation they cannot be split, nonlinear Froude-Krylov and hydrostatic loads and nonlinear water-on-deck and slamming loads if these local phenomena are excited. One must note that the retardation functions associated with the convolution integrals are as for a purely linear system, which means that they can be obtained either from the linear added-mass or from damping coefficients at all frequencies. The same is true for the instantaneous hydrodynamic loads connected with infinite-frequency added mass. This means that these hydrodynamic coefficients can be found using a frequency-domain solver. Within this weak-scatterer seakeeping solver, only the body-boundary condition needs to be satisfied at any time instant, while the free-surface boundary condition is implicitly enforced on $z = 0$. It leads to a great reduction in terms of computational cost. Moreover, also the loads with nonlinear effects need to be estimated in time and the equations of motion need to be integrated.

In particular, the motion equations are solved in time by a fourth-order Runge-Kutta scheme. When evolving from time t to $t + \Delta t$ the water-on-deck loads, the slamming loads and the convolution integral terms, are estimated in t and retained constant during the time interval Δt. The other loads are estimated at any time instant required by the scheme. The convolution integrals are evaluated by using a step-wise linear interpolation of the involved functions and then integrating analytically along each time step. The computational cost is limited by estimating the convolution integrals only in the time interval where the retardation functions are non zero. For the ship and incident waves examined here, this time interval is much lower than ten incident-wave periods. The most time consuming element of the solver is represented by the water-on-deck solution, which has not been parallelized yet.

The developed solver can handle ship interactions with regular linear and weakly-nonlinear waves and with long-crested irregular waves through superposition principle. It can examine both ships at rest and with a limited forward

speed, using the approach in [13]. The assumption of small vessel speed is suitable in the case of large wave-induced ship motions possibly leading to water on deck and/or slamming. Indeed, in such conditions it is expected that the ship master would reduce the speed.

The roll-damping coefficient predicted from the free decay tests on the FPSO model has been introduced in the related equation of motion to account for corrections from viscous effects, though in this case they are very limited as mentioned in the previous section and verified in [4]. In a similar manner other hydrodynamic loads estimated from the model tests, and not predictable by the potential-flow solver, can be included to assess their relevance and consequences on the vessel behavior. This has been used in the analysis discussed in the next section.

4. Physical investigation

Here the experiments and numerical results are compared and used to carry on a physical investigation of the vessel in waves.

Parametric-roll and water-on-deck occurrence. Tables 1 and 2 examine the parametric-roll (PR) and water-on-deck (WOD) occurrences caused, respectively, by incident waves with $\beta = 180^\circ$ and 175° from experiments and numerical simulations. For cases with PR the roll amplitude is given as predicted and measured, complemented by the standard deviation for the experimental data. For cases with WOD the boolean 'YES' is used because no measurements of level or amount of shipped water was done in the tests. The incident-wave parameters are given in terms of the prescribed incident-wave steepness kA and of the prescribed wavelength-to-ship length ratio λ/L and the corresponding calm-water roll natural frequency-to-excitation frequency ratio ω_{4n0}/ω. Both ratios are reported because λ/L is relevant for water-on-deck occurrence while ω_{4n0}/ω is of interest for parametric-roll excitation. The actual generated waves were slightly different from the prescribed conditions and were reproduced numerically for comparison. The correspondence between the prescribed and actual values for each incident-wave case can be found in table 3 while here for convenience the nominal values are considered. In the tables, 'X' indicates cases not studied experimentally because too dangerous and so neither reproduced numerically. Concerning the water on deck, 'NI' for the experiments means that the water shipping was observed but not periodically, *i.e.* not at every incident-wave period T, and was small. For the numerical water-on-deck events 'NI' means that those events were associated with very small amount of shipped water; in particular it corresponds to an averaged water level on the deck less than 2 mm and 0.7 mm, respectively, for $\beta = 180^\circ$ and 175° when expressing the values in model scale. From the water-on-deck tables, both experimental and numerical results indicate WOD occurrence for $kA >= 0.2$ in both heading conditions and for any value of λ/L. The numerics slightly overestimates the occurrence of WOD for sufficiently small kA. This could be reasonably explained by wave-body nonlinear effects missing in the numerical modelling which matter more for the local flow evolution, due to greater sensitivity, when the incident-wave nonlinearities are not strong enough. For $\beta = 175^\circ$, the limit of WOD occurrence tends to slightly enlarge with respect to head-sea conditions in the plane (λ/L, kA) for intermediate λ/L values. For this heading angle, incident waves with $kA = 0.2$ and $\lambda/L = 0.75$ cause water

Table 1: $\beta = 180°$: Occurrence of parametric-roll resonance (PR, left) and water on deck (WOD, right) for the cases studied experimentally and reproduced numerically. For cases with parametric resonance it is reported the roll amplitude complemented by the standard deviation for the measurements. For incident waves with $\lambda/L = 1$ and $kA = 0.1$ experimentally PR did not reach the steady-state conditions during the recorded time history, therefore the maximum roll amplitude is provided. This is also reported for the numerics, while the second numerical prediction for this case corresponds to the steady-state PR amplitude.

$\lambda/L \rightarrow$	0.75	1.00	1.25	1.50	2.00	0.75	1.00	1.25	1.50	2.00
$\omega_{4n0}/\omega \rightarrow$	0.402	0.464	0.519	0.568	0.656	0.402	0.464	0.519	0.568	0.656
Method kA	PR					WOD				
Exper. 0.10	NO	21.3°±0.3°	NO	NO	NO	NO	NO	NO	NO	NO
Num 0.10	NO	19.3°/16.2°	NO	NO	NO	NO	NO	NO	NO	NO
Exper. 0.15	NO	15.4°±0.3°	NO	NO	NO	NO	NO	NI	NO	NO
Num 0.15	NO	13.2°	NO	NO	NO	NO	NI	NI	NO	NO
Exper. 0.20	26.7°±0.4°	NO	NO	NO	X	YES	YES	YES	YES	X
Num 0.20	24.6°	8.4°	NO	NO	X	YES	YES	YES	YES	X
Exper. 0.25	27.2°±0.4°	NO	NO	NO	X	YES	YES	YES	YES	X
Num 0.25	23.1°	NO	NO	NO	X	YES	YES	YES	YES	X

Table 2: $\beta = 175°$: Occurrence of parametric-roll resonance (PR, left) and water on deck (WOD, right) for the cases studied experimentally and reproduced numerically. For cases with parametric resonance it is reported the roll amplitude complemented by the standard deviation for the measurements. For incident waves with $\lambda/L = 1.25$ and $kA = 0.25$ experimentally two runs were done, runs 44 and 46, respectively, without and with PR occurrence, as reported here.

$\lambda/L \rightarrow$	0.75	1.00	1.25	1.50	2.00	0.75	1.00	1.25	1.50	2.00
$\omega_{4n0}/\omega \rightarrow$	0.402	0.464	0.519	0.568	0.656	0.402	0.464	0.519	0.568	0.656
Method kA	PR					WOD				
Exper. 0.10	NO	17.9°±1.7°	NO	NO	NO	NO	NO	NO	NO	NO
Num 0.10	NO	15.9°	NO	NO	NO	NO	NO	NO	NO	NO
Exper. 0.15	NO	16.4°±1.3°	NO	NO	NO	NO	NI	NI	NI	NO
Num 0.15	NO	11.3°	NO	NO	NO	NO	YES	YES	NI	NO
Exper. 0.20	26.3°±0.4°	9.5°±2.0°	NO	11.3°±3.7°	X	due to PR	YES	YES	YES	X
Num 0.20	25.0°	6.3°	NO	NO	X	due to PR	YES	YES	YES	X
Exper. 0.25	25.3°±1.6°	NO	NO/12.1°±3.7°	12.9°±2.08°	X	YES	YES	YES	YES	X
Num 0.25	21.8°	NO	NO	NO	X	YES	YES	YES	YES	X

on deck only as a consequence of a parametric-roll occurrence. This is clear both from the experimental video and from the numerical prediction of the shipped water (see figure 3), because in both cases no WOD is recorded when the heave and pitch motions are already large and nearly in steady-state oscillations. The water shipping occurs only

Table 3: Correspondence between prescribed and actual incoming-wave parameters in terms of wavelength-to-ship length ratio and steepness. The first value given is kA and the second λ/L.

$\lambda/L \rightarrow$	0.75	1.00	1.25	1.50	2.00	0.75	1.00	1.25	1.50	2.00
kA	$\beta = 180°$					$\beta = 175°$				
0.10	0.10/0.75	0.10/1.00	0.10/1.25	0.10/1.50	0.10/2.00	0.11/0.76	0.10/1.00	0.12/1.28	0.13/1.49	0.11/2.03
0.15	0.15/0.75	0.15/1.00	0.15/1.25	0.15/1.50	0.15/2.00	0.17/0.76	0.17/1.00	0.17/1.29	0.17/1.50	0.15/2.00
0.20	0.21/0.76	0.20/1.00	0.20/1.25	0.20/1.50	0.20/2.00	0.22/0.76	0.21/1.00	0.21/1.28	0.22/1.49	X
0.25	0.25/0.75	0.25/1.00	0.25/1.25	0.25/1.50	0.25/2.00	0.25/0.76	0.26/1.00	0.21/1.28	0.26/1.29	X

Figure 3: Nominal incident waves with $\lambda/L = 0.75$ and $kA = 0.2$. Left and center: experimental snapshots before (left) and after (center) PR occurrence at the time instants with largest relative vertical motion at the bow. Right: numerical pitch, roll and WOD occurrence as a function of time.

after the roll resonance has been established with sufficiently high oscillation amplitude. Moreover, numerically no water shipping is predicted when the roll motion is restrained (not given here).

Concerning the parametric roll, the experiments show a more profound difference for the two heading conditions. In head-sea conditions experimental and numerical results indicate PR occurrence for the two lowest ω_{4n0}/ω values, *i.e.* $\omega_{4n0}/\omega \simeq 0.402$ and 0.464, which are close and smaller than the frequency ratio at the first parametric resonance. This suggests that, close to the first parametric resonance, shorter incident waves are more dangerous for PR occurrence. For $\omega_{4n0}/\omega \simeq 0.402$, PR occurs only for sufficiently large kA while the opposite is true for $\omega_{4n0}/\omega \simeq 0.464$. Because larger incident-wave nonlinearities lead usually to higher nonlinear effects in the wave-body interactions, this would suggest that nonlinear wave-body interactions effects support PR for sufficiently short incident waves and bring out of the resonance for larger incident wavelengths. Numerical and experimental PR estimates are consistent but for $\omega_{4n0}/\omega = 0.464$ and $kA = 0.20$ where the model tests do not record any PR while the numerics predicts a PR with a steady-state roll amplitude $\xi_{4a} \simeq 8.4°$. Such value is limited relative to the other cases of parametric roll recorded numerically and experimentally, where ξ_{4a} ranged between about 13° to more than 20°. This would suggest that the examined incident-wave condition could be close to the limit of PR occurrence and so the approximations in the DD solver in reproducing the nonlinear wave-body interaction effects could be more relevant for the numerical solution.

With $\beta = 175°$, for sufficiently small steepness the experiments show PR occurrence only at $\omega_{4n0}/\omega = 0.464$, as in head sea. From table 2, at this frequency ratio nonlinear effects tend to avoid the parametric resonance but the avoidance of parametric resonance requires higher steepness than in head sea. Similarly as for $\beta = 180°$, at smaller ω_{4n0}/ω the nonlinear effects bring the ship in resonance condition for $kA \geq 0.2$. For larger ω_{4n0}/ω the vessel behavior shows differences with respect to the head-sea condition. In particular, increasing the frequency ratio, nonlinear effects tend to destabilize the system and the minimum kA value for PR resonance reduces. This is in contradiction with what observed in head-sea conditions (see table 1) where the nonlinearities tend to avoid PR for increasing ω_{4n0}/ω. Moreover, such features are not shown by the numerical results which only predict PR at the two lowest ω_{4n0}/ω examined, with a trend consistent with the experiments.

Yaw-roll coupling for the FPSO: experiments. The reason for the mentioned PR occurrences recorded in the tests at $\beta = 175°$ was found through a detailed investigation of the case with $\omega_{4n0}/\omega = 0.519$ and $kA = 0.25$. The ship interaction with this incident wave was examined twice (runs 44 and 46) because of a set-up problem during the first run performed, and opposite results in terms of parametric resonance were recorded in the two cases. Consistently with the numerics, the first run (run 44) was not associated with PR and produced large amount of WOD (see left plot of figure 4). Important amount of liquid entered the vehicle and produced a change in the hydrostatic properties

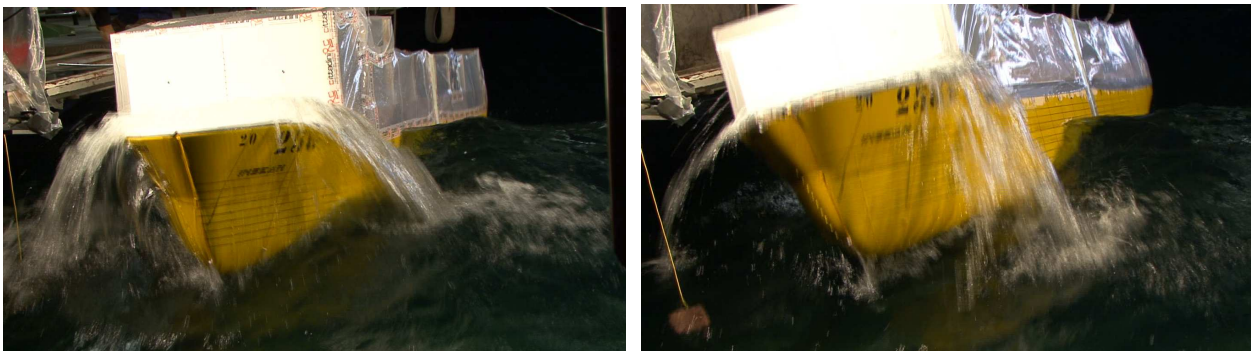

Figure 4: Nominal incident waves with $\omega_{4n0}/\omega = 0.519$ and $kA = 0.25$: run 44 (left) and run 46 (right) at the time instant with wave crest at mid-ship.

of the vessel. This is confirmed by the behavior of the recorded heave (ξ_3) and pitch (ξ_5) ship motions showing a drift in time which means an increase of the instantaneous draft and a progressive bow-down evolution (see top plots of figure 5). The ship experiences very limited roll (ξ_4, whose amplitude was about 3°) and the yaw (ξ_6) was very small and at most 3 degrees, though ideally it should be zero (bottom plots of figure 5). To make sure that this type of accident would not happen again, the model was suitably dried and made waterproof and the test was repeated as run 46. In this case PR occurred, as well as important WOD (see right plot of figure 4) but without any leakage of liquid inside the model. So, as expected, no drift occurred for heave and pitch while their amplitudes of oscillations appeared similar as for run 44 (top plots of figure 5). The occurrence of parametric roll is accompanied by larger yaw motion with a non regular behavior and with amplitudes exceeding 5 degrees (bottom plots of figure 5). The different

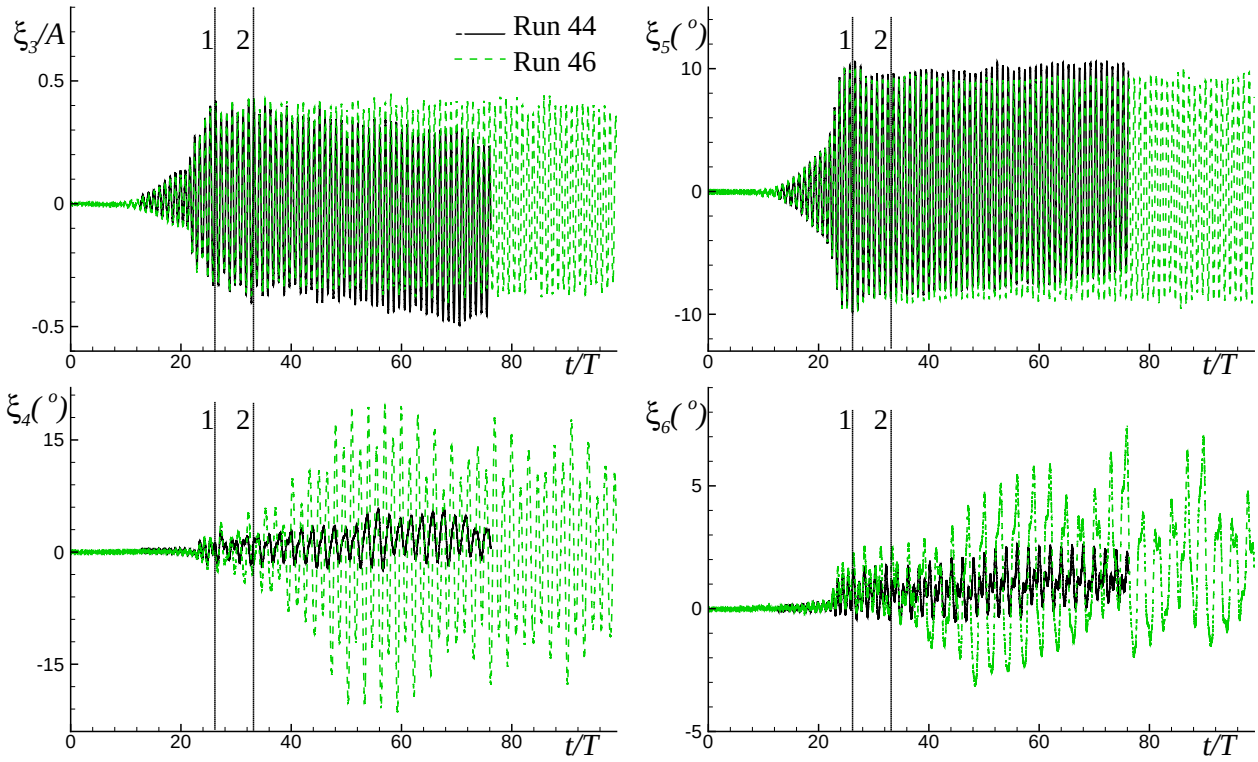

Figure 5: Nominal incident waves with $\omega_{4n0}/\omega = 0.519$ and $kA = 0.25$: heave (top-left), pitch (top-right), roll (bottom-left) and yaw (bottom-right) motions for run 44 and run 46. Heave is positive upwards and positive pitch means bow down. Vertical dotted lines in the plots indicate roughly the time when yaw and roll for runs 44 and 46 show clear differences (1) and when the drift starts to characterize heave and pitch (2).

behavior between runs 44 and 46 in terms of roll and yaw occurs before the drift starts to affect the heave and pitch motions for run 44 (please compare vertical dotted lines indicated as 1 and 2 in figure 5). This means that the leakage of water inside the ship is not the reason for preventing PR and larger yaw motion for run 44.

The different observed behavior motivated a more in-depth analysis of the experiments. Checking the 3D videos from the model tests the reason for the larger yaw motion was found to be reasonably connected with some slack of the shaft used to ideally block such motion. This discovered experimental problem highlighted an important effect of the coupling between roll and yaw on the parametric-roll occurrence and features. Indeed the roll oscillation amplitude exceeds 15 degrees for run 46.

Then the yaw-motion time histories for all examined waves were examined to check the shaft effectiveness. Before the accident, the shaft worked sufficiently well for waves with $\omega_{4n0}/\omega \leq 0.519$ at any steepness, with yaw oscillation amplitudes well below 2 degrees, while longer incident waves represented a challenge for the shaft and the higher kA the shorter becomes the time interval required to build up non-negligible yaw oscillations. The accident made just less effective the shaft and so the slack was more pronounced. As a consequence also at $\omega_{4n0}/\omega = 0.519$ and $kA = 0.25$ the yaw was not so limited when the test was repeated. Figure 6 shows the yaw and roll evolutions for cases with nominal frequency ratio $\omega_{4n0}/\omega = 0.568$ and $kA \geq 0.15$. From the measurements, the lowest steepness is

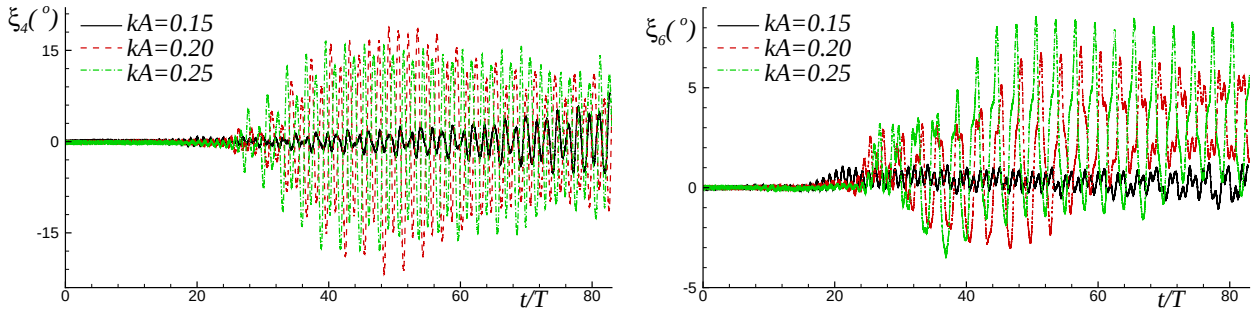

Figure 6: Nominal incident waves with $\omega_{4n0}/\omega = 0.568$ and $kA = 0.15$, 0.20 and 0.25: experimental roll (left) and yaw (right) motions.

associated with a very slow development of yaw-roll coupling which leads only at the end of the recordings to a visible increase of the roll and the appearance of a lower frequency of oscillation relative to the incident-wave frequency ω. Contemporary the yaw shows clearly a two-frequency content, *i.e.* the incident-wave frequency and an oscillation frequency equal to the yaw natural frequency. Because of such weak trend to instability, this incident-wave case was classified as without parametric resonance. The two steepest waves are instead clearly associated with roll instability, with amplitudes exceeding 15 degrees and apparently correlated with sufficiently large yaw oscillations.

Since run 46 highlighted the occurrence of a yaw-roll coupling due to slack in the shaft and the subsequent large roll oscillations, this case was used as sample condition to investigate more in detail the features of yaw-roll coupling. Figure 7 splits in four parts the roll and yaw time evolutions (left panels) and provides for each the corresponding phase plots (right panels). During the first stage (first row), linear effects dominate and both motions oscillate with the incident-wave period; then (second row), ξ_6 acquires a chaotic behavior with a global trend to increase the period of oscillation, its coupling with ξ_4 leads to a reduction in the roll period from $2T$ (first parametric roll resonance) to $1.5T$. In the third phase (third row), the roll period is dominated by $1.5T$ and the yaw becomes a regular motion with dominant period equal to $3T$, i.e. twice the roll period. ξ_4 is modulated in time by the yaw period $3T$. As a result, essentially two modes are well visible in the corresponding roll phase plot. In the last stage (fourth row), the yaw motion is again characterized by a chaotic regime and the yaw-roll coupling appears dominated by nonlinear effects.

Yaw-roll coupling for the FPSO: simplified 2-dof system. Due to the strong nonlinearities expected in the yaw restoring caused by the slacked shaft, it is not easy to reproduce numerically similar conditions for further investigation. But an attempt is done in the following with the aim to gain insights about the nature of the coupling. Because the sway in the experiments was restrained and it was assessed to be very small from the measurements, it is assumed a 2-dof roll-yaw linear system in steady-state resonant conditions of the form

$$\begin{aligned}(I_{44} + A_{44})\ddot{\xi}_4 + A_{46}\ddot{\xi}_6 + B_{44}\dot{\xi}_4 + B_{46}\dot{\xi}_6 + C_{44}\xi_4 + C_{46}\xi_6 &= F_{exc,4}\\ A_{64}\ddot{\xi}_4 + (I_{66} + A_{66})\ddot{\xi}_6 + B_{64}\dot{\xi}_4 + B_{66}\dot{\xi}_6 + C_{64}\xi_4 + C_{66}\xi_6 &= F_{exc,6}\end{aligned} \tag{1}$$

It means that the restoring loads connected with yaw and roll are linearized and assumed connected with constant coefficients, which is a rough simplification. On the other hand it would not be straightforward to identify the explicit

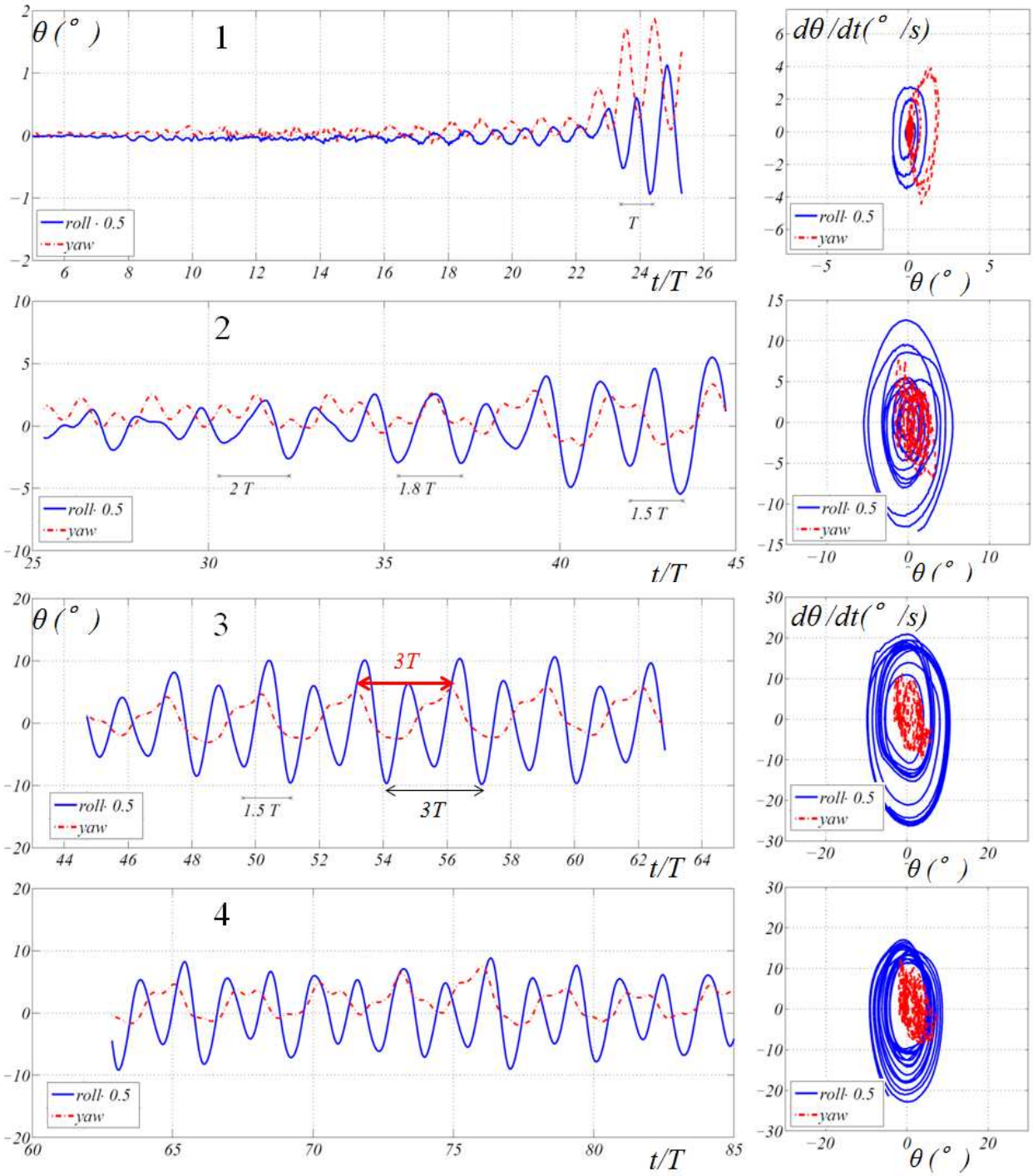

Figure 7: Nominal incident waves with $\omega_{4n0}/\omega = 0.519$ and $kA = 0.25$: run 46. Four stages (increasing from top to bottom) of the roll and yaw motions (left panels) and the corresponding phase plots (right panels).

nonlinear mathematical form of the involved hydrodynamic loads. Moreover, as the roll damping also the yaw damping and the cross-coupling damping terms are taken as linear. To study the behavior of this system we need to know all

terms involved. Here this is done considering measurements for run 46 and in particular those within the time interval of the motion evolution in which the yaw is dominated by the sub-harmonic oscillation period $3T$ and the roll by $1.5T$, which are assumed to be coincident with their natural periods in coupled conditions. This hypothesis is confirmed by the DD numerical simulations in the later figure 8. The peculiar links of these periods to the incident-wave period suggests that, similarly as for parametric roll without yaw, also this roll-yaw instability could be associated with specific incident wave-to-natural frequency ratios. Since the added-moment and damping coefficients depend on the frequency, here they are assumed at the yaw natural frequency. It is also reasonably assumed that $B_{64} = B_{46}$ and $C_{64} = C_{46}$. The inertial and added-moment terms are known, respectively, from the vessel properties and from the frequency-domain radiation solution at the yaw natural frequency. C_{44} is evaluated from its definition and C_{66} and C_{64} are obtained knowing the natural frequencies for roll and yaw modes of the coupled system and assuming them as natural frequencies in undamped conditions. This implies neglecting the variation with the damping. The damping in roll is evaluated from the free-decay tests, as explained in section 2, while B_{66} and B_{64} are tentatively estimated using the fact that $F_{exc,6}$ was measured by a torque sensor during the tests and applying an identification process. The latter is performed enforcing that the recorded yaw moment in the right-hand side of the second equation of (1) equals the left-hand side with unknowns only the damping coefficients. Such identification procedure is one of the weakest parts in this analysis since the yaw and roll velocities are not in phase. Especially for B_{64} the results might be affected by large error. As discussed later in the text, the DD numerical simulations showed that using the sixty percent of the value identified for this damping coefficients provides numerical motions more consistent with the experiments. Therefore this corrected value has been applied in the following analysis.

Yaw-roll coupling for the FPSO: numerical and experimental analysis. The coefficients B_{66}, $B_{46} = B_{64}$, C_{66} and $C_{46} = C_{64}$, identified from the experiments and through assuming a 2-dof yaw-roll coupled system, were introduced in the equations of motions of the DD solver and the yaw motion was also included in the numerical analysis. It means that the wave interactions with a 4-dof FPSO were simulated. It was found that the estimated value of $B_{46} = B_{64}$ was too large, *i.e.* it leads to much larger roll and yaw motions than experimentally. More consistent predictions were obtained considering the sixty percent of this value. The results of the simulations are given in figure 8 in terms of heave, pitch, roll and yaw motions, together with the corresponding predictions assuming zero yaw and with the measurements of run 46 during the third phase of the evolution, *i.e.* the one with yaw dominated by the period $3T$ and roll dominated by the period $1.5T$ (see figure 7). From the comparison, as expected the heave and pitch motions are not much affected by the inclusion of yaw motion in the simulations. Moreover the roll motion from the prediction including ξ_6 is consistent with the measurements in particular both in terms of involved oscillation frequencies and amplitudes. The yaw motion is not far from the experimental behavior but the amplitudes involved are overestimated. This suggests difficulties in recovering adequately the nonlinear restoring loads and the yaw-related damping due to the shaft action. However it confirms the yaw and roll oscillation periods, respectively, $3T$ and $1.5T$ as their coupled natural periods. Indeed the nonlinear roll restoring is calculated by the numerical method, *i.e.* not enforced from

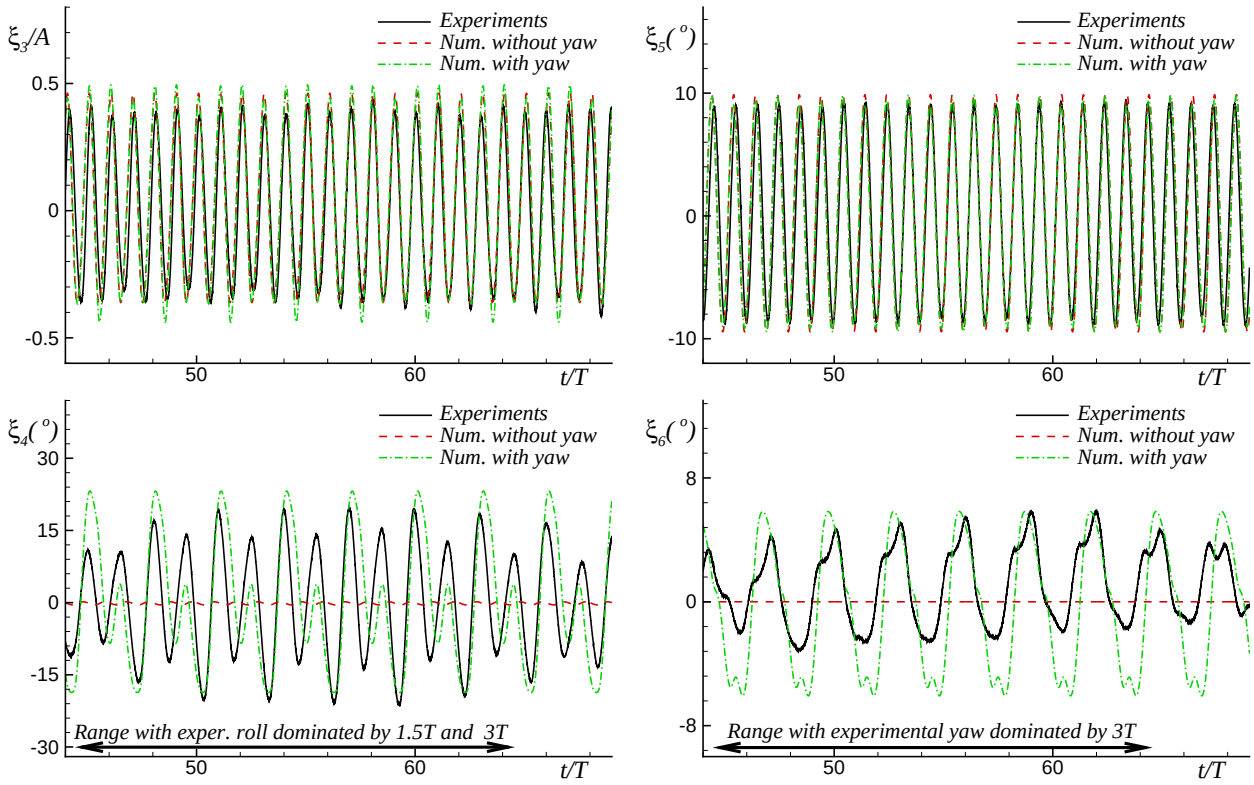

Figure 8: Nominal incident waves with $\omega_{4n0}/\omega = 0.519$ and $kA = 0.25$: heave (top-left), pitch (top-right), roll (bottom-left) and yaw (bottom-right) motions for run 46 and obtained numerically by the DD solver without and with yaw motion.

the linearized 2dof system, and leads to capture a roll oscillation period of $1.5T$ as in the experiments. This supports the idea that it must be a feature of the system and indicates a resonance condition in these incident waves. The quantitative comparison is better documented by figure 9 showing the frequency content of the numerical steady-state roll and yaw together with the corresponding data in the third phase of the experimental evolution. The numerics predicts correctly the frequency content in both motions, it overestimates the contribution in the roll connected with the modulation frequency $f = 1/3T$ which appears of similar importance as $2/(3T)$ while is much more limited for the experiments. The predictions also overestimate the contributions of $1/3T$ and $2/(3T)$ to the yaw. Both numerics and experiments show a limited contribution connected with the incident-wave frequency, *i.e.* $f = 1/T$.

This analysis confirms that the yaw-roll coupled motion plays the most important role in the parametric resonance of roll for this case and shows that the use of the simplified 2-dof coupled system, to provide needed information to the DD solver, served the scope of capturing such instability. On the other hand one can expect that nonlinear effects matter substantially.

The DD solver is used next to further investigate the role played by motions coupling and load nonlinearities in the parametric-roll occurrence of run 46. In particular the role of load nonlinearities can be assessed by switching on and off the nonlinear effects in the different loads of interest, *i.e.* setting to zero the nonlinear contributions modelled

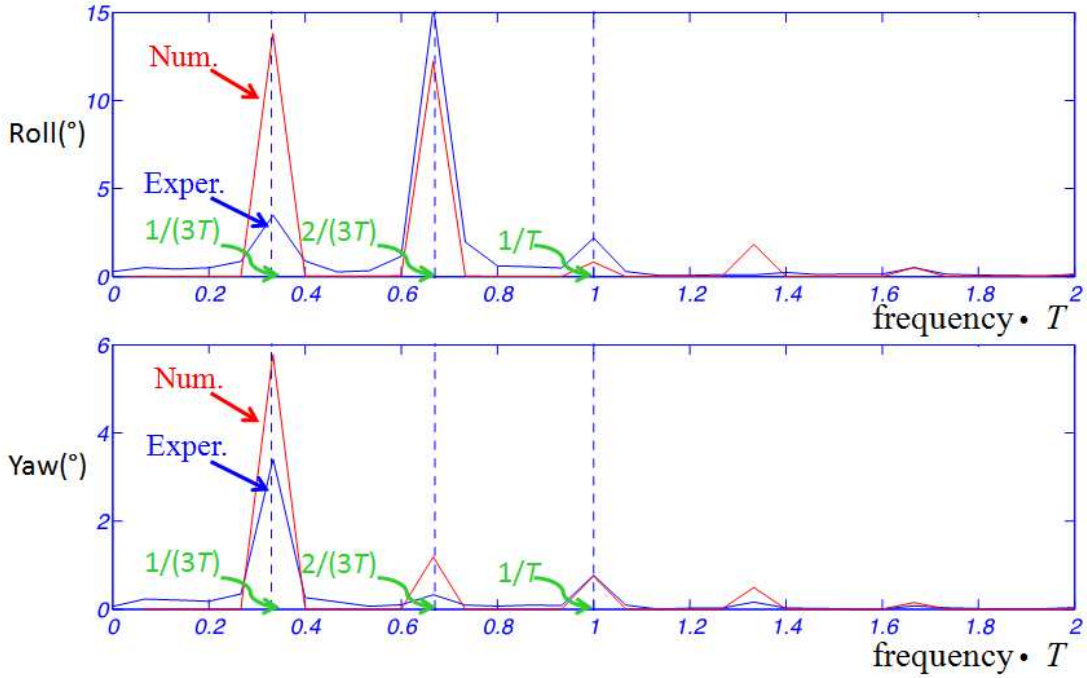

Figure 9: Nominal incident waves with $\omega_{4n0}/\omega = 0.519$ and $kA = 0.25$: frequency content of roll (top) and yaw (bottom) in numerical steady-state conditions and in stage 3 of the experimental evolution (see figure 7).

numerically. The main results are summarized in the left tables of figure 10. As obvious result, it is found that no parametric roll is excited when the roll restoring moment is estimated as linear. When roll hydrostatic load is taken as nonlinear, there is an instability but the steady-state roll amplitude is limited. Large roll amplitude, more consistent with the measurements, can be achieved considering nonlinear hydrostatic loads also for the other motions. Comparing the yaw and roll results for such cases (right plots of figure 10), we see that they are similar in terms of oscillation amplitudes but one must remember that the coupling of roll and yaw by itself is essential for the parametric-roll occurrence since, with restrained yaw, no instability is excited for this incident-wave case.

It is interesting to note that also the later stages of the recorded evolutions for nominal incident waves with $\omega_{4n0}/\omega = 0.568$ and $kA = 0.15$, 0.20 and 0.25 (see figure 11) show that the yaw oscillation period tunes to $3T$, with T the incident-wave period. This is barely visible for the results with lowest steepness and actually in this case such oscillation period is first shorter and slightly increases in time relative to the results for the two other incident waves. This aspect is not shown in the enlarged view of this figure, but it can be checked examining the whole time histories in figure 6. In addition, for all cases this motion is also characterized by the incident-wave period T. The roll is dominated by an oscillation period around $1.5T$ for all cases and reduces as kA increases likely because of nonlinear effects in the roll restoring, though one cannot exclude possible experimental errors. One must note that, for sake of clarity, the yaw motions were synchronized so to have the first indicated peak at the same time instant for all three cases and the roll motions were shifted consistently.

Linear Pitch and heave

Yaw \ Roll	Linear	NonLinear
Linear	NO	Small
NonLinear	NO	– – Large

NonLinear Pitch and heave

Yaw \ Roll	Linear	NonLinear
Linear	NO	— Large
NonLinear	NO	– · Large

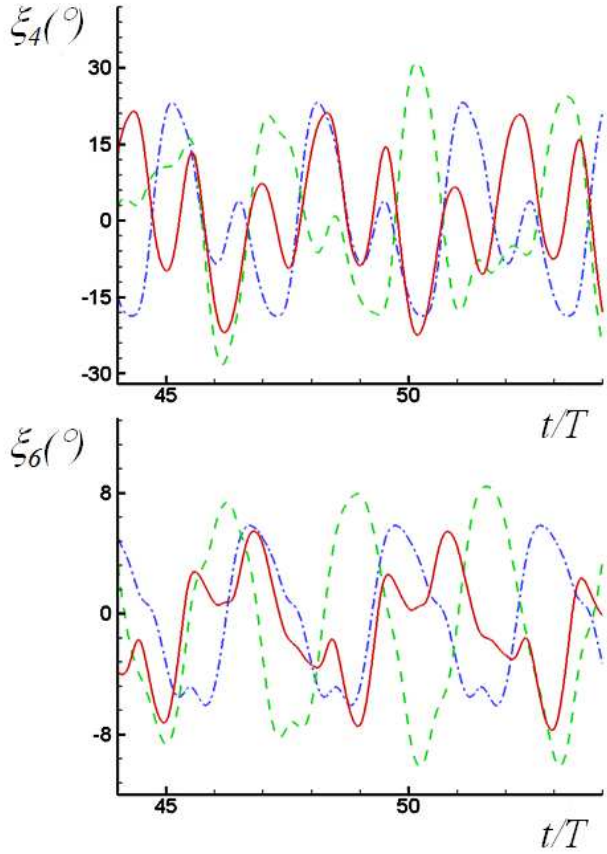

Figure 10: Nominal incident waves with $\omega_{4n0}/\omega = 0.519$ and $kA = 0.25$: influence of nonlinearities in the hydrostatic loads for heave, pitch, roll and yaw on the roll instability. Left: table with linear and nonlinear effects in roll and yaw considering linear (top) and nonlinear (bottom) effects in heave and pitch. Right: roll (top) and yaw (bottom) time histories for the results with relevant roll instability.

If we simulate these incident-wave conditions just using in the DD solver the hydrodynamic coefficients as found for run 46, we predict a yaw-roll coupling but overestimate the occurrence of instability and the amplitudes for the two motions, especially for $kA = 0.15$ (see figure 12). Moreover, the oscillation periods for the yaw are nearly $3T$, but the oscillation periods for the roll are not captured. This is because the linearized coefficients B_{66}, $B_{64} = B_{46}$, C_{66} and $C_{64} = C_{46}$ are set as for run 46 but the incident-wave frequency is different. So the damping coefficients can be different, since they are in general frequency dependent, and also the restoring coefficients can be different, since they depend in general on the involved nonlinear motion-coupling effects. To reproduce these cases numerically in a more correct way, we should estimate the values of the equivalent linear coefficients C_{66}, $C_{46} = C_{64}$, B_{66} and $B_{46} = B_{64}$ in these conditions, similarly as done for run 46. Such an approach is not pursued here because will not add anything to what already discovered and documented. As noted for run 46, one must stress that this type of analysis would lead to a simplified model of the system because of the linearization of the hydrodynamic coefficients. On the other hand, as already mentioned, it is hard to perform a nonlinear investigation and the proposed approach represents a first attempt with promising outcomes.

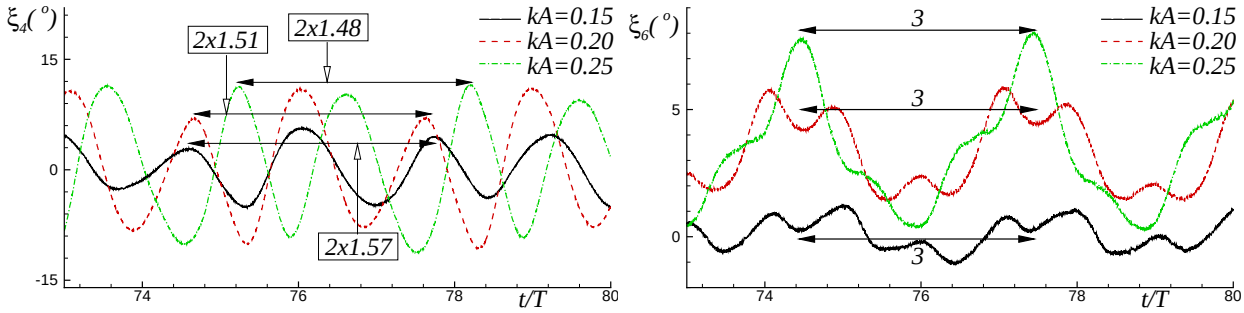

Figure 11: Nominal incident waves with $\omega_{4n0}/\omega = 0.568$ and $kA = 0.15$, 0.20 and 0.25: experimental roll (left) and yaw (right) motions at the later stages of the evolution.

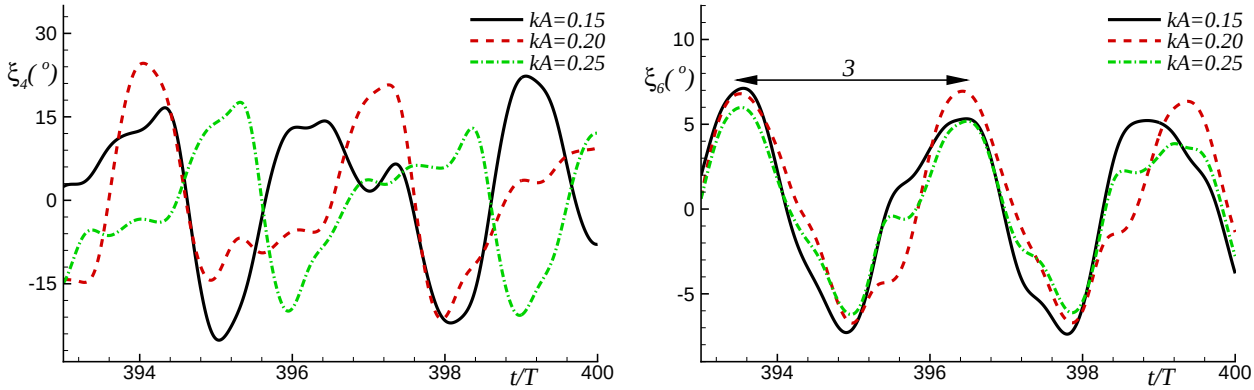

Figure 12: Nominal incident waves with $\omega_{4n0}/\omega = 0.568$ and $kA = 0.15$, 0.20 and 0.25: roll (left) and yaw (right) motions at the later stages of the evolution as predicted by the DD solver using the yaw-related hydrodynamic coefficients estimated for run 46.

Yaw-roll coupling for the FPSO: consequences on water on deck. The detailed investigation presented in [4] for the same FPSO ship in head-sea conditions, and so without yaw excitation, showed that the occurrence of parametric roll tends to increase the amount of shipped water and to make more severe the water on deck in terms of induced pressure on the deck. Using the same numerical solver, here the effect of roll instability connected with yaw-roll coupling is examined for nominal incident waves with $\omega_{4n0}/\omega = 0.519$ and $kA = 0.25$. The results are reported in figure 13 in terms of volume of shipped water (left plot) and pressure at a location on the deck (center plot) shown in the right sketch of the figure. This location is very close to the deck superstructure and the predicted pressure peak corresponds to an equivalent water column of about 8 m at full scale for the case without yaw, while it is almost halved with yaw-roll coupling. Similarly, the maximum volume of shipped water without yaw corresponds to an average level of liquid on the deck of about 2.7 m at full scale, while it reduces to about 1.7 m with yaw-roll coupling.

Also the experiments indicate qualitatively a larger amount of shipped water for run 44, *i.e.* with very small yaw, with respect to run 46. This is documented in figure 14. Two snapshots are shown for each run, respectively, at the later stage of the water-on-deck phase (still persisting for run 44 and practically over for run 46) and at the early stage of the water-off-deck phase. The images for run 44 refer to time instants before the drift appears in heave and pitch motions due to the water leakage inside the model; those for run 46 correspond to the phase when roll instability

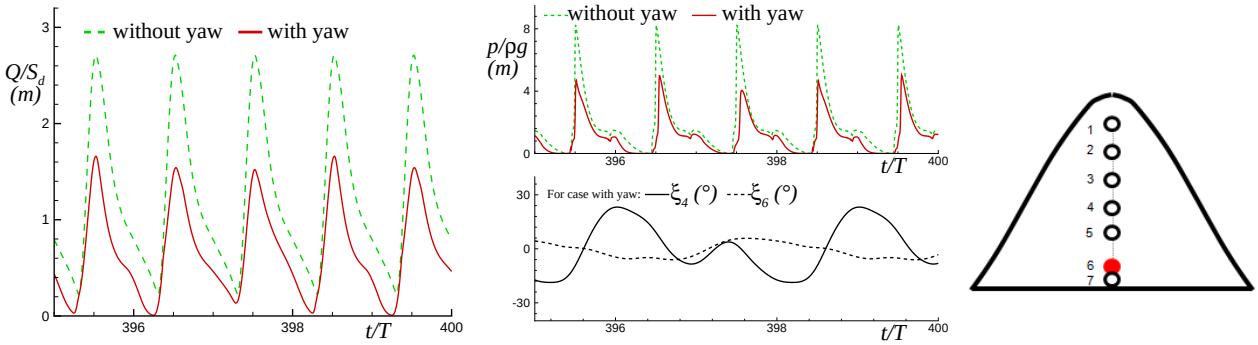

Figure 13: Nominal incident waves with $\omega_{4n0}/\omega = 0.519$ and $kA = 0.25$ without and with yaw motion: evolution in the steady-state regime for the volume of shipped water (left) and for the pressure (center) at a deck location indicated by the full circle in the right sketch. Here S_d is the area of the deck. The volume of water is given as averaged liquid height on the deck at full scale and the pressure as equivalent height of liquid column at full scale.

is well established. Especially the first snapshots (left part of the figure) highlight that the amount of liquid on the deck for run 44 when the water-shipping is not finished yet is larger than that associated with run 46 for which the water shipping is already ended. According to the numerical investigation, also for the incident-wave cases with $\omega_{4n0}/\omega = 0.568$ and $kA = 0.15$, 0.20 and 0.25 the severity of the water shipping reduces when the yaw motion is not restrained and modelled using the hydrodynamic coefficients identified for run 46 (not shown here).

These results suggest that the yaw-roll coupling and related instability phenomenon tend to work against the water shipping, differently from what observed in head-sea conditions, *i.e.* without yaw motion, where PR tends to support the water on deck.

Yaw-roll coupling for the FPSO: influence of slamming loads. The numerical simulations for run 46 performed with and without bottom-slamming model suggest a negligible effect of slamming loads on the occurrence and features of roll-yaw instability for this case. However the measurements of the pressure on the hull bottom have not been analyzed yet. This is left for a future step of the research and is important to validate quantitatively the numerical predictions of slamming occurrence and subsequent loads for this case and so to support these numerical findings.

Yaw-roll coupling for other ships. It would be relevant to investigate the role of the yaw-roll coupling in the excitation of motion instabilities also for other ship geometries. In this framework, a recent numerical study on a fishing vessel has been performed in [14] as preliminary assessment of an experimental set-up for parametric-roll investigations. The numerical method is the same as the one adopted in the present analysis. In this case the fishing vessel is assumed connected to four cables to limit the horizontal vessel motions. In the ship mean configuration, these cables are horizontal and symmetric with respect to the vessel longitudinal axis. The focus is on the effects of different rigid degrees of freedom and their coupling on parametric-roll occurrence. The model and the sketch of the planned set-up are provided in figure 15. When the yaw motion is allowed, the yaw-roll coupling appears important and tends to promote motion instability. This is examined in figure 16 in terms of roll and yaw time histories induced by

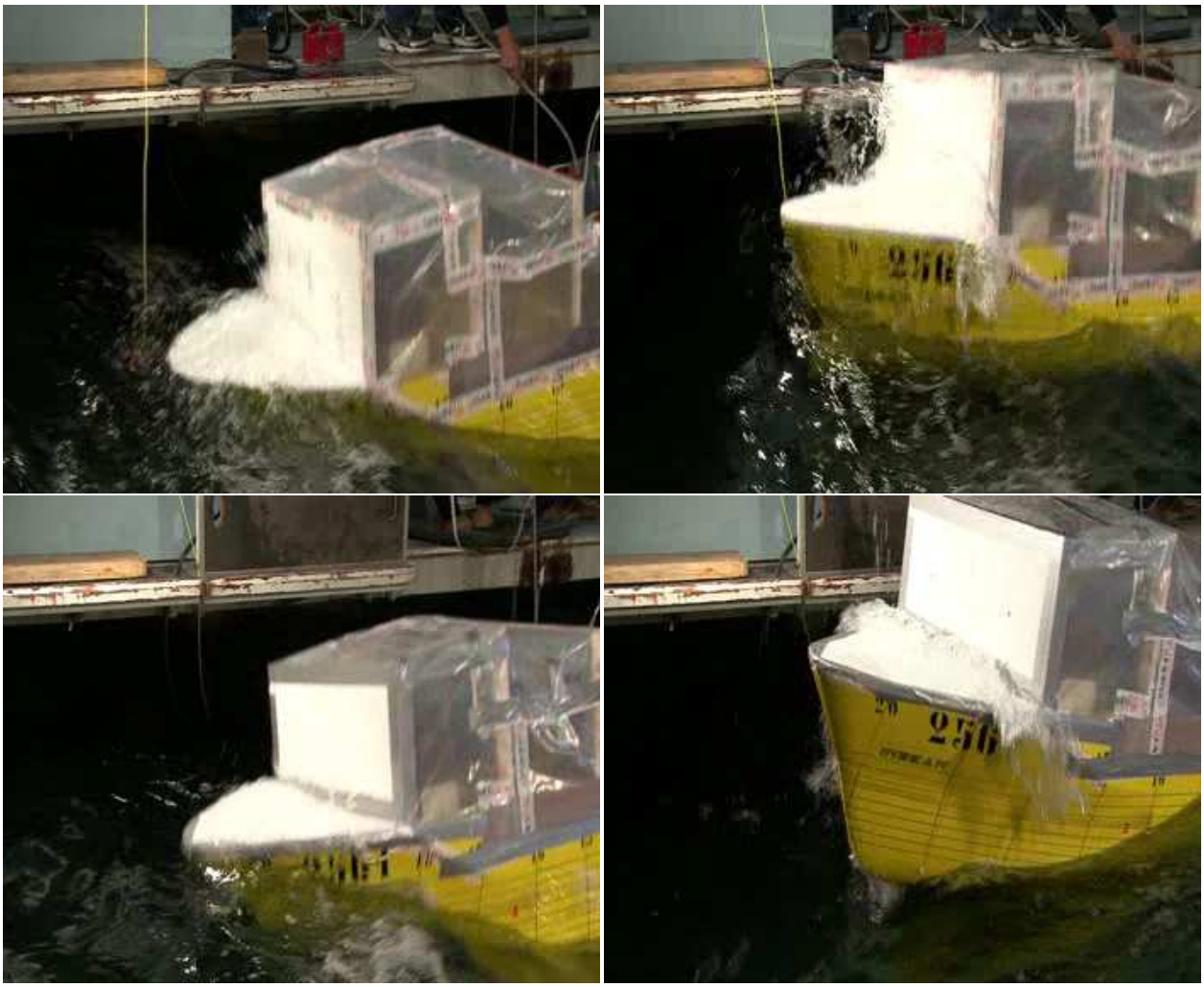

Figure 14: Nominal incident waves with $\omega_{4n0}/\omega = 0.519$ and $kA = 0.25$: run 44 (top) and 46 (bottom). Left: late stage of water-on-deck phase. Right: early stage of water-off-deck phase.

regular incident head-sea waves with $\omega_{4n0}/\omega = 0.47$ and $kA = 0.25$. No viscous damping effects are accounted for in the simulations and the sway motion is restrained. From the results, at first (1) the yaw motion oscillates at its natural frequency induced by the linear-restoring from the cables, while the roll is negligible; then (2) PR is excited by the wave-body interaction, ξ_4 oscillates at a period $2T$ and the yaw shows also an additional higher frequency superimposed to its natural frequency, with the latter about twice the roll frequency. The roll-yaw coupling leads (3) ξ_6 to oscillate with the same frequency as the roll, but eventually (4) the yaw goes back to its natural frequency (changed by the coupling with roll) and induces a reduction in the roll oscillation period. This process leads to a progressive increase of the two motion amplitudes until the break-down of the simulation. The latter is prevented when viscous damping, as estimated from free decay tests, is introduced for the yaw in the simulations, while accounting for the experimental damping in surge and roll does not avoid the solution blow up. This confirms the role of yaw in destabilizing the system. Compared with the same incident-wave case but with fixed yaw, the roll-yaw coupling

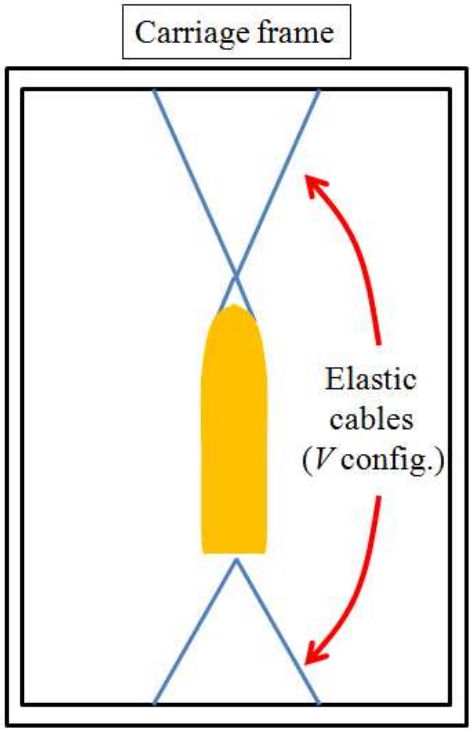

- With cables
- Surge
  +Yaw
  +Sway

Length (L)	2.95 m
Breadth (B)	0.95 m
Draft (D)	0.4 m
Displacement	0.622 ton
Pitch Gyration radius	0.28 L
Roll Gyration radius	0.38 B
Metacentric height (GM)	0.082 m

Figure 15: Fishing vessel: ship model in scale 1:10 and related hydrostatic properties and experimental conditions (left) and top-view sketch of the cables system to be used(right).

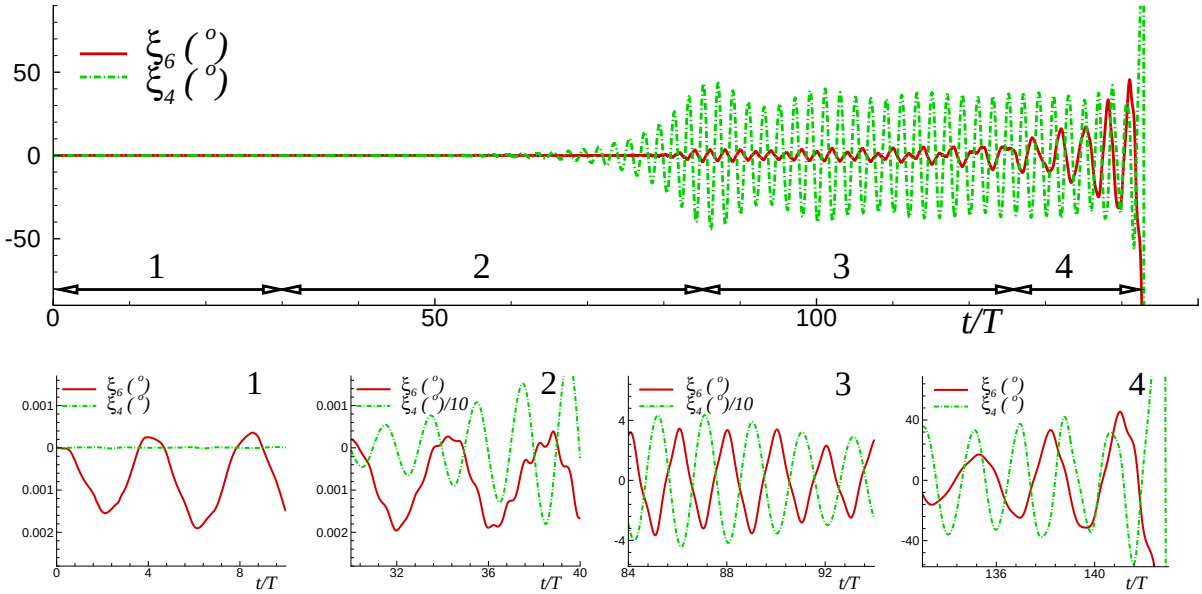

Figure 16: Fishing vessel in regular head-sea wave (ω_{4n0}/ω = 0.47, kA = 0.25). Overall (top) and zoomed views (bottom) of the numerical time histories of the roll and yaw motions.

promotes more rapidly the parametric resonance.

In the case of the fishing vessel, the yaw restoring is provided by the cables and so more linear and with much lower value than the yaw restoring in our FPSO case which is linked to the shaft slack. This can explain the different features in terms of temporal development of the yaw-roll coupling and oscillation periods involved. Nevertheless the two cases present important similarities since their related analyses suggest that the roll-yaw coupling is dangerous for the parametric roll in head or bow sea and, as the yaw motion becomes sufficiently large, tends to reduce the roll natural oscillation period (see the zoomed view labelled as 4 in the figure) from his initial value of $2T$ which corresponds to the first roll-parametric resonance. This means that the use of a proper control system is crucial not only for directional stability but also for parametric-roll resonance.

5. Conclusions

A combined experimental and numerical investigation has been carried out on the occurrence of parametric roll and water on deck in bow-sea regular waves close to head sea for a FPSO ship, *i.e.* with $\beta = 175°$. The main focus was on the roll instability phenomenon. Experimentally, the wave-body interactions were examined in terms of induced ship motions, video recordings of the vessel and possible water shipping events, and measurements of other relevant variables. The numerical solver is based on a Domain-Decomposition strategy using a weak-scatterer potential-flow seakeeping solver, a shallow-water approximation for water possibly shipped onto the deck and a local Wagner-type of solution for possible bottom-slamming events.

From the investigation, the small variation in heading angle, relative to the head-sea condition, is not much relevant for the water-shipping occurrence while the parametric roll indicates instability also in longer waves when the involved steepnesses are sufficiently large. This feature is not captured by the numerical simulations which assume restrained yaw motion as ideally enforced in the tests. Besides this the numerics globally agrees with the experiments. A closer view to the model tests highlighted problems in the effectiveness of the shaft aimed to stop the yaw motion so that non negligible yaw oscillations occur in waves long enough and with sufficiently large steepness. The yaw-roll coupling is then excited and this seems to promote the instability of the system and can also change the natural frequency of the roll. In particular, it tends to reduce it. The yaw-roll coupling and related instability also affect the water-on-deck phenomenon with the tendency in reducing its severity. This is opposite to the influence of the parametric roll when the yaw is null, as documented in [4]. As expected, for the roll instability the nonlinearities in the roll restoring moment are essential but the nonlinearities in the restoring of the other involved motions play also a role. The yaw-roll coupling seems to be relevant for the instability excitation also for other vessels and it would be interesting to further investigate this aspect in the future with the aim of identifying critical operational conditions.

The global comparison between experiments and DD results indicate a possible use of this numerical method not only for head-sea conditions but also for bow-sea conditions. A next step of the numerical development is to extend the method to short-crested waves with main direction at $\beta = 180°$.

Acknowledgment

This research activity is partially funded by the Centre of Excellence CeSOS, NTNU, Norway, partially by the Research Council of Norway through the Centres of Excellence funding scheme AMOS, project number 223254, and partially by the Flagship Project RITMARE - The Italian Research for the Sea - coordinated by the Italian National Research Council and funded by the Italian Ministry of Education, University and Research within the National Research Program 2011-2013.

References

[1] O. M. Faltinsen, Hydrodynamics of High-Speed Marine Vehicles, Cambridge University Press, Cambridge, UK, 2005.

[2] M. Neves, C. Rodriguez, On the assessment of parametric rolling of ships in head seas, in: C. G. Soares, Y. Garbatov, N. Fonseca, A. Teixeira (Eds.), Marine Technology and Engineering, 2011, pp. 563–573.

[3] M. Greco, C. Lugni, Numerical and experimental study of parametric roll with water on deck, in: Proc. of Int. Conference on Violent Flows (VF-2012), Nantes, France, 2012.

[4] M. Greco, , C. Lugni, O. M. Faltinsen, Can the water on deck influence the parametric roll of a fpso? a numerical and experimental investigation, European Journal of Mechanics - B/Fluids 47 (2014) 188–201.

[5] M. Greco, C. Lugni, O. Faltinsen, Roll-yaw coupling effects on parametric resonance for a ship in regular waves, in: Proceedings of 29th International Workshop of Water Waves and Floating Bodies, Osaka, Japan, 2014.

[6] M. Greco, C. Lugni, 3-d seakeeping analysis with water on deck and slamming. part 1: numerical solver, Journal of Fluids and Structures 33 (2012).

[7] Z. Q. Zhou, J. Q. De Kat, B. Buchner, A nonlinear 3-d approach to simulate green water dynamics on deck, in: Piquet (Ed.), Proceedings of 7th International Conference of Numerical Ship Hydrodynamics, Nantes, France, 1999, pp. 5.1–1, 15.

[8] E. Toro, Godunov Methods: Theory and Applications, Kluwer Academic/Plenum Publishers, 2001.

[9] G. Colicchio, Violent disturbance and fragmentation of free surfaces, Ph.D. thesis, University of Southampton, Southampton, UK, 2004.

[10] H. Wagner, Uber stoss- und gleitvorgange an der oberflache von flussigkeiten, ZAMM 12 (1932) 192–235.

[11] J. Pawlowski, A theoretical and numerical model of ship motions in heavy seas, in: SNAME Transactions, volume 99, 1991, pp. 319–315.

[12] W. Cummins, The impulse response function and ship motions, Symposium on Ship Theory, Schiffstechnik 9 (1962) 101–109.

[13] N. Salvesen, E. O. Tuck, O. M. Faltinsen, Ship motions and sea loads, SNAME Transactions 78 (1970) 250–287.

[14] M. Greco, C. Lugni, Numerical study of parametric roll on a fishing vessel, in: 32nd Int. Conference on Offshore Mechanics and Arctic Engineering (OMAE'13), Nantes, France, 2013.